Characterization of spatial heterogeneity in groundwater applications

PhD Thesis

Department of Geotechnical Engineering and Geo-Sciences (ETCG)

Technical University of Catalonia, UPC

Paolo Trinchero

February 2009

HYDROGEOLOGY GROUP
TECHNICAL UNIVERSITY OF CATALONIA

Chapter 2

Point-to-point connectivity: what we can infer from pumping and tracer tests*

2.1 Introduction

Although in the last twenty years many efforts have been devoted to define and assess the impact of hydraulic connectivity in groundwater flow and solute transport, limited visible results are appreciable in raising the policy makers and the consultancy actors awareness of its importance in risk assessment studies. The main reasons can be associated to the non unique definition of connectivity and the lack of a more comprehensive mathematical framework.

First evidences of the role of connectivity in flow and transport processes arose in the 1980s with the blossoming of groundwater studies in fractured media. A key idea was highlighted by

*This chapter is based on the article: Trinchero, P., X. Sanchez-Vila, and D. Fernandez-Garcia (2008), Point-to-point connectivity, an abstract concept or a key issue for risk assessment studies?, *Advances in Water Resources*, *10.1016/j.advwatres.2008.09.001*.

de Marsily [21] who argued that only a small subset of the fractures were actually contributing to total flow and transport. The idea was soon tranfered to porous media. *Fogg* [32] carried out a numerical study of the three-dimensional distribution of hydraulic conductivity, K, in the Wilcox aquifer system. He argued that the flow system in the aquifer was mainly controlled by the continuity and interconnectedness of the sand, rather than by their actual local hydraulic conductivity values. *Poeter and Townsend* [74] studied a two-dimensional section of a fluvial aquifer having highly connected hydraulic features. They found that the travel time estimates exclusively calculated based on the effective conductivity associated with extreme values were more consistent with field observations. *Fogg et al.* [33] characterized a fan aquifer using hydrostratigraphic analysis. Although the channel facies were not extensively connected, their stochastic model indicated that facies with high K-values fully percolated the domain in all three dimensions. In a later work, *LaBolle and Fogg* [56] showed that connectivity of low-permeability hydrofacies is an important process controlling the migration of contaminant plumes and the success of remediation actions.

Sanchez-Vila et al. [82] analyzed the departure from the assumption of multiGaussianity in mapping the spatial variations of aquifer properties through geostatistical theories. They found that the presence of structures favoring connectivity of the large local T values yields effective transmissivity values, T_{eff}, larger than the geometric mean, T_G, the latter value being the effective transmissivity in multiGaussian 2-D fields.

The impact of connectivity of extreme transmissivity values on solute transport was investigated by *Gomez-Hernandez and Wen* [38], who found that the assumption of multiGaussianity could largely underestimate travel times. This assumption was further explored by *Zinn and Harvey* [105]. Well connected fields were found to enhance Darcy-scale mass transfer processes in the system producing tailing in the breakthrough curves, while disconnected fields displayed macrodispersivity values smaller than those observed for multiGaussian fields. Moreover their results regarding effective conductivity reproduce those of *Sanchez-Vila et al.* [82]. *Zheng and Gorelick* [103] studied the effect of having a synthetic fracture network of narrow channels with

high conductivity embedded in a homogeneous porous medium. When the contrast of permeability between the channel and the matrix was larger than 100, the spatial concentration of the plume exhibited high asymmetrical non-Gaussian features. On the contrary, when the contrast of permeability was reduced to 30 : 1, the solute plume approached a Gaussian behavior. High connected flow paths have been shown numerically to lead to power-law type breakthrough curves [e.g., 1, 57, 101].

Western et al. [100] argued that the classical geoestatistical methods based on two-point statistics are not able to capture most of the important connectivity features occurring in natural formations, i.e., preferential flow channels. The reason is that the variogram, which has a central role in geostatistics, accounts for the differences of the variable between two points separated at a fixed distance, but does not consider the values located between these two points. To overcome this problem, the authors proposed the use of connectivity functions which measure the probability that two separate points are connected by a continuous path. Still, their statistical approach is based on some visual inspection of the geological features and does not include the driven physical processes of flow and transport. In the same context, recently *Kerrou et al.* [50] assessed the performance of stochastic multiGaussian techniques to preserve connectivity patterns when characterizing a non multiGaussian braided channel aquifer. In agreement with *Western et al.* [100], their results emphasized the need for an adequate description of connectivity, which is not captured by two-point statistics. Another recent line of work consists in defining the random functions by means of multiple-point geostatistics [89, 53].

A different, albeit related concept, is connectivity of systems based on percolation theory [5, 8, 72, 61, 20]. In these works, connectivity has a clear physical meaning indicating whether a given fluid is capable of flowing from one point (surface) to another. This process is characterized by the potential existence of a connecting path (classical percolation theory) potentially coupled with the availability of the fluid to invade that particular path (invasion percolation theory). No connection would in a sense mean that there are areas with null transmissivity, and connectivity becomes a

geometrical feature. Our work focuses on a different approach, since we consider a continuous porous medium, where connectivity is a relative process (”better” or ”worse”) indicating whether it is possible to connect two points through a path where at all points T is large compared to some reference value.

In a recent study, *Knudby and Carrera* [51] numerically tested several intuitive indicators of flow and transport connectivity aiming at discerning between well connected and disconnected fields as a whole. They found a weak correlation between flow and transport indicators. Later on, the same authors [52] analyzed the use of apparent diffusivity, D_r (estimated transmissivity divided by estimated storage coefficient), as a measure of connectivity using a Monte Carlo analysis. They found that D_r has a certain degree of correlation with indicators of both transport and flow global connectivity.

As evidenced by this brief review, in the last decades a great effort has been dedicated to the study of connectivity as a global property of the field or as an intrinsic feature of fractured systems. Few studies focus on the impact of connectivity patterns on pumping or tracer tests in which the velocity of the signal (heads or concentrations) response between two distinct points is crucial. *Schad and Teutsch* [85] inferred information on the effective length scale of the heterogeneity structure using pumping test data. *Meier et al.* [62] analyzed numerically the meaning of the parameters obtained when interpreting a pumping test by the Cooper-Jacob method [15] in heterogeneous confined aquifers. For low to moderate degrees of heterogeneity, they found that the estimated transmissivity, T_{est}, was close to the geometric mean of the transmissivity field, while the estimated storage, S_{est}, could significantly vary with the observation location, being indicative of the hydraulic connectivity between the observation location and the pumping well. These results were confirmed analytically by *Sanchez-Vila et al.* [83] who obtained an approximated analytical expression for S_{est} by truncation of an infinite series solution.

Fernandez-Garcia et al. [29] analyzed a suite of breakthrough curves obtained from convergent flow tracer tests in an anisotropic heterogeneous medium that was reconstructed in the lab-

oratory. They found that the arrival time (or the estimated porosity) of breakthrough curves was primarily controlled by the preferential flow paths occurring between the pumping well and the injection location, providing little information on the global properties of the transmissivity field, i.e., T_{eff}. Thus, their results gave an explanation for the observed discrepancy between porosity estimates obtained from field tracer tests and their representative values. This explanation had already been hinted by *Sanchez-Vila and Carrera* [80] in their analysis of a tracer test performed in a highly heterogeneous strongly anisotropic medium.

An issue to be considered when addressing point-to-point connectivity is the local effect of drilling at the pumping well location. If the well is located in a distinct (high or low) T area, including the possibility of skin effects or perturbations from the drilling process, the signal towards the injection or observation well would be remarkably different. This effect has been studied by *Butler* [11] in confined aquifers and by *Trinchero et al.* [93] in leaky aquifers.

The lack of a proper understanding of point-to-point connectivity in a more quantitative manner has prevented its use in many field applications. In particular, proper understanding of connectivity will benefit and improve available methods used to delineate capture zones or perimeter protection areas in heterogeneous aquifers. Still, a large number of publications have addressed the topic indirectly by means of ensembles averages of numerical Monte Carlo simulations [86, 97, 14, 40, 77].

This paper focuses on the meaning of point-to-point connectivity under convergent flow conditions. Specifically, we evaluate analytically the relationship between two indicators of point-to-point connectivity: the storage coefficient estimated using the Cooper-Jacob method [15], S_{est}, which is an indicator of flow connectivity and measures the velocity of the hydraulic response, and the estimated porosity, ϕ_{est}, which is an indicator of transport connectivity and measures the characteristic advective travel time. The approximate analytical solution is tested against synthetic and laboratory experiments, and provides a clear explanation for the observed weak correlation between flow and transport connectivity indicators [51]. Our solution allows the direct delineation

of connectivity patterns based on some knowledge of the transmissivity field in many practical applications, such as delineation of capture zones.

2.2 Field and Laboratory Evidences

2.2.1 Pumping tests

The hydraulic response of pumping tests has been frequently observed in the field to substantially vary with the observation location. Figure 2.1 shows the time-drawdown data of a pumping test performed in a fractured media in Southern Spain. Drawdown data were measured in three different piezometers and each time-drawdown curve was interpreted separately using the Cooper-Jacob method. In short, this well-Known method consists in plotting the drawdown versus log-time curve. The transmissivity, T_{est}, is obtained from the late-time slope of the drawdown curve, m, and the storage coefficient, S_{est}, is obtained from the time at which the projection line of the slope intercepts the zero drawdown axis, t_0,

$$T_{est} = 0.183\frac{Q}{m}, \tag{2.1}$$

$$S_{est} = \frac{2.25 T_{est} t_0}{r^2}. \tag{2.2}$$

We note that while the late-time slope of the drawdown curves depicted in Figure 2.1 are almost the same for the three piezometers, a large variability is observed in the hydraulic response, having P3 the fastest response. The corresponding estimated parameters are shown in Table 6.1. We emphasize that while T_{est} is almost constant for all observations, S_{est} varies up to two orders of magnitude. *Meier et al.* [62] attributed these large variations in S_{est} to a good hydraulic connectivity between the pumping well W and the piezometer P3 and a relatively bad hydraulic

connectivity between the well and piezometers P1 and P2. These connectivity features are actually clearly visible in this particular site by mapping the geologic lineaments which follow the N-NW direction. The same authors reported several aquifers in the world where this effect of constant T_{est} and variable S_{est} was observed.

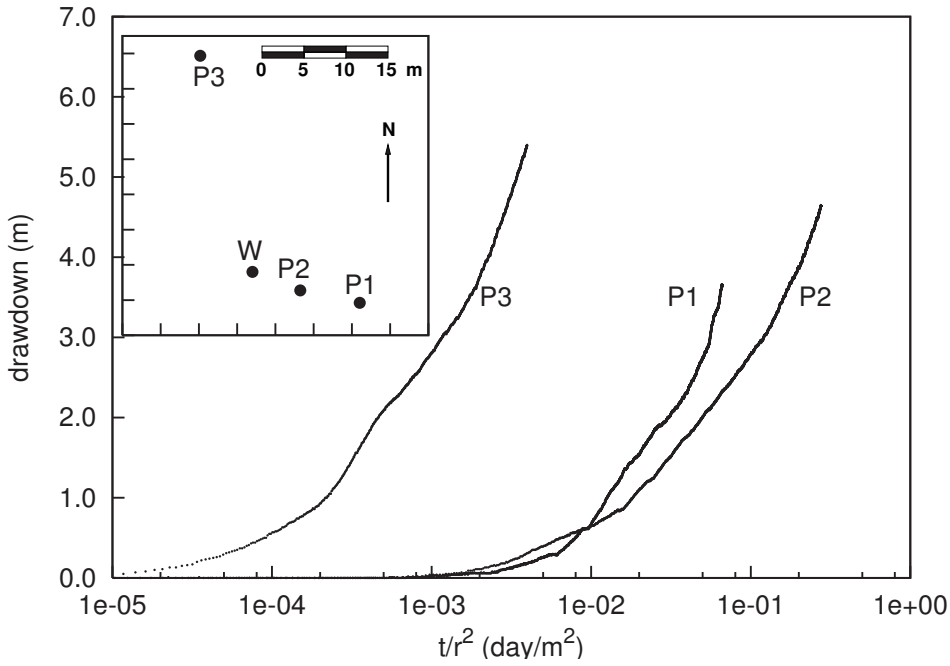

Figure 2.1: Drawdown curves of a pumping test performed in a fractured media in Spain. In the small box it is represented the space location of the well, W, and the three piezometers, P1, P2 and P3. In a homogeneous medium the three curves would collapse.

The observed impact of connectivity on S_{est} was formally expressed by *Sanchez-Vila et al.* [83], who derived an analytical solution for S_{est} upon considering a spatially varying transmissivity. Then, by truncation of an infinite series expansion, they found an approximate expression for S_{est} given by

$$S_{est}(r_o, \theta_o) = S \exp\left(-\frac{1}{\pi}\int_0^{2\pi}\int_0^{\infty} Y'(\rho,\varphi)\, U(r_o,\theta_o,\rho,\varphi)\, d\rho d\varphi\right), \tag{2.3}$$

where S is the actual storage coefficient representative of the aquifer system (assumed constant), $Y'(\mathbf{x}) = \ln(T(\mathbf{x})/T_0)$, $T(\mathbf{x})$ is the point value of transmissivity at the $\mathbf{x}$ location, T_0 is the effective aquifer transmissivity, (ρ, φ) are the polar coordinates centered at the pumping well, (r_o, θ_o) is the observation location in polar coordinates, and $U(r_o, \theta_o, \rho, \varphi)$ is a weighting function defined as

$$U(r_o, \theta_o, \rho, \varphi) = -\frac{\rho - r_o cos(\theta_o - \varphi)}{(\rho^2 + r_o^2 - 2\rho r_o cos(\theta_o - \varphi))\rho}. \tag{2.4}$$

This expression not only agrees with field observations in that S_{est} varies with the observation location, but further describes the dependency of S_{est} on the transmissivity features by means of a weighted spatial integral over the entire space. The role of connectivity appears directly in the formulation. In fact from the shape of the weighting function, depicted in Figure 2.2, we see that large transmissivity values (larger than T_0) located between the well and the observation point leads to S_{est} smaller than S and vice versa.

Table 2.1: Interpretation of the pumping test of figure 2.1 using the Cooper-Jacob method.

	$T_{est}(m^2/day)$	S_{est}
P1	$2 \cdot 10^{-1}$	$4 \cdot 10^{-2}$
P2	$3 \cdot 10^{-1}$	$2 \cdot 10^{-2}$
P3	$3 \cdot 10^{-1}$	$3 \cdot 10^{-4}$

2.2.2 Laboratory Tracer Tests

Field tracer tests constitute a valuable tool to estimate the governing parameters of solute transport in an aquifer. Known chemical species (tracers) are carefully added into the system and monitored with time and/or with space. Among all configurations, convergent flow tracer tests are typically preferred for simplicity. In this case, once quasi steady state flow conditions are established, the tracer is injected at a point located several meters away from a well that is pumped at a constant rate. Concentrations with time (breakthrough curve) are measured at the pumping well. Then,

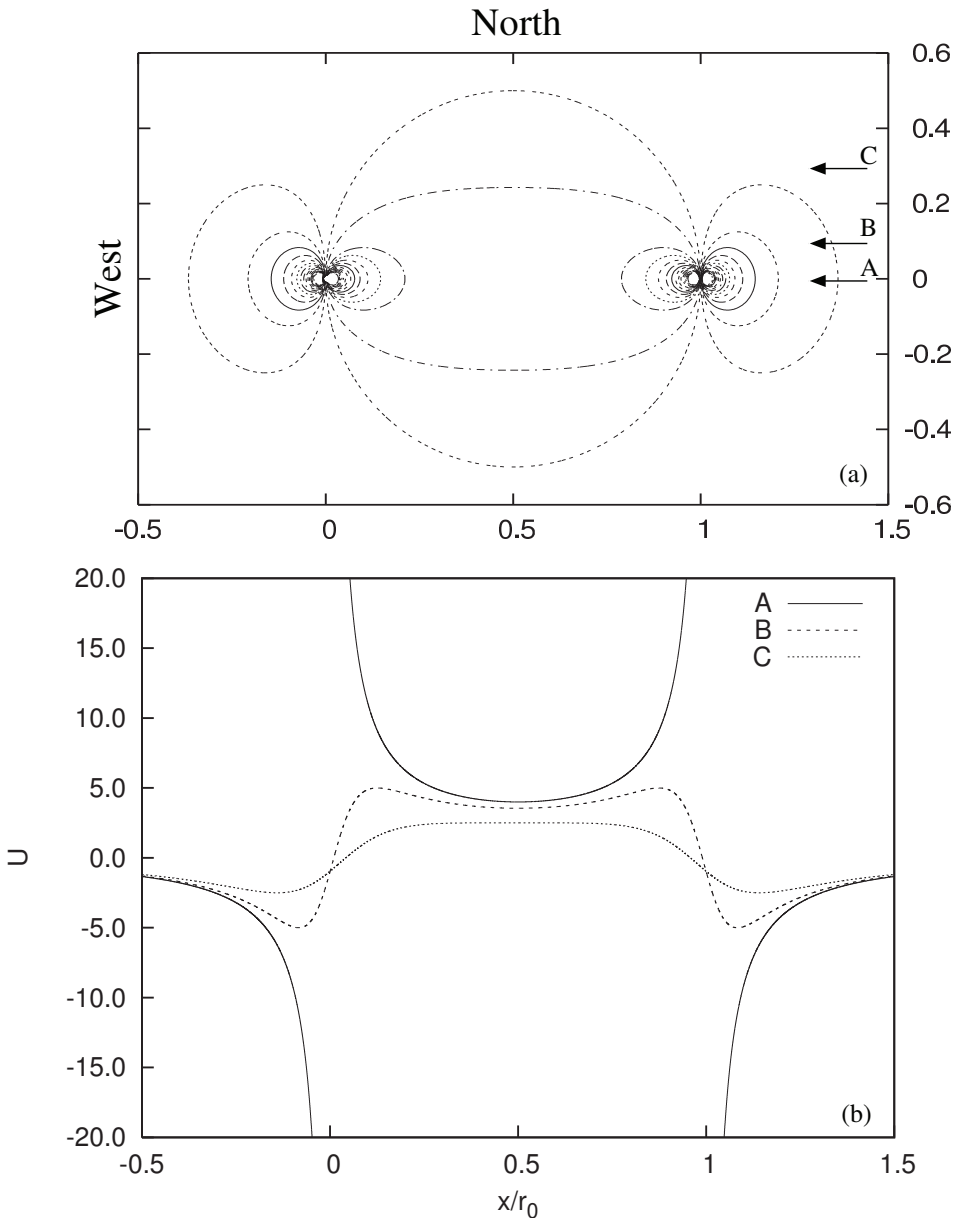

Figure 2.2: Shape of the weighting function $U(r_o, \theta_o, \rho, \varphi)$ (Equation 2.4) (a) and profile along the indicated sections (b) for a well located in the origin $(0, 0)$ and a observation point in $(1, 0)$. $U(r_o, \theta_o, \rho, \varphi)$ is positive inside the circle defined by the pumping and observation well, and negative outside (being 0 along the circle itself). The points corresponding to the two wells are singular.

transport parameters are typically obtained by curve-fitting the tracer breakthrough curve with a known homogeneous transport model solution. Additionally, porosity estimates can also be determined from the advective travel time of the solute tracer, t_a, as

$$\phi_{est} = \frac{Q_w t_a}{\pi\left(r_i^2 - r_w^2\right)} \tag{2.5}$$

where r_i is the radial distance between the pumping well and the tracer injection location, r_w is the well radius, and Q_w is the pumping rate per unit of thickness. If not obtained from the curve-fitting procedure, t_a can also be estimated by the mean arrival time or the first normalized temporal moment of the breakthrough curve,

$$t_a = \frac{\int_0^\infty tC(t)dt}{\int_0^\infty C(t)dt} \tag{2.6}$$

Connectivity has been observed to largely influence the porosity estimates, ϕ_{est}, obtained from (2.5). We refer to these effects as transport point-to-point connectivity. Although these effects are routinely observed in the field, the analysis of connectivity based on field data is cumbersome because of a limited number of available tracer experiments and large uncertainties inherent to the depiction of the heterogeneous formation.

In this context, intermediate-scale laboratory tracer experiments performed in reconstructed aquifers provide valuable information to study the processes governing connectivity under well controlled conditions. In the laboratory, perfect knowledge of the physical system and numerous tracer experiments can be feasibly achieved. *Fernandez-Garcia et al.* [29] investigated transport connectivity in a reconstructed anisotropic two-dimensional heterogeneous aquifer in the laboratory. The physical system was created packing together sand lenses of different conductivities in a horizontal sand box of size 243.8 cm $\times$ 121.9 cm. Five different sands were used. Figure 2.3 depicts the spatial distribution of the different sands along with the injection locations that were used

to conduct convergent-flow tracer tests with Sodium Bromide. Corresponding Bromide breakthrough curves are summarized in Figure 2.4. Here, we present their results using a dimensionless time to highlight the striking differences that were observed relative to the behavior of a homogeneous porous medium. In the homogeneous case, all breakthrough curves should exhibit the same shape with a center of gravity located at $t_D = 1.0$. The authors found that the mean travel time reflected in an individual breakthrough curve mostly depends on the particular hydraulic features existing between the pumping well and the injection location, thereby providing little information on the global properties of the aquifer (see Figure 2.4), but interesting information regarding point-to-point connectivity.

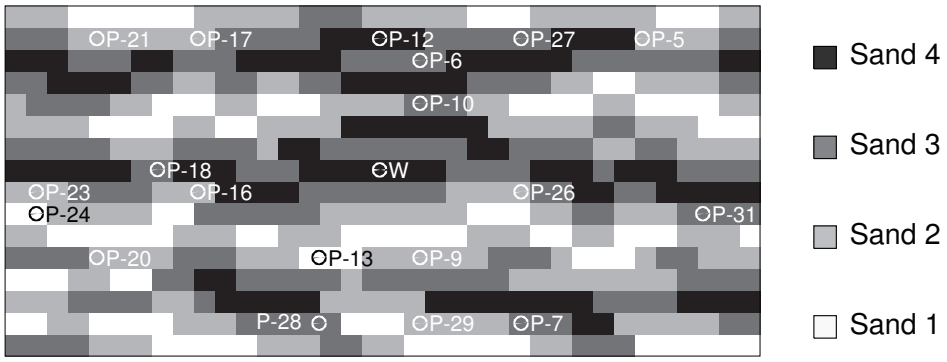

Figure 2.3: Transmissivity field of the sand box and location of the ports. Four sand types were used, dark indicating higher transmissivity values ($62m^2/day$, $22m^2/day$, $7m^2/day$ and $2m^2/day$ respectively). The position of the well (W) and the observation points or ports (P) are indicated.

2.3 Analytical Relationship Between ϕ_{est} and S_{est}

As stated in the previous section, the two connectivity indicators, ϕ_{est} and S_{est}, provide a different measure of connectivity. In this section we explore whether it is possible to relate them. In the following we consider a two-dimensional porous media under convergent flow conditions induced by a pumping well in an otherwise static pressure aquifer system. Boundaries are considered to be located sufficiently far from the area of study so that their impact upon drawdown is negligi-

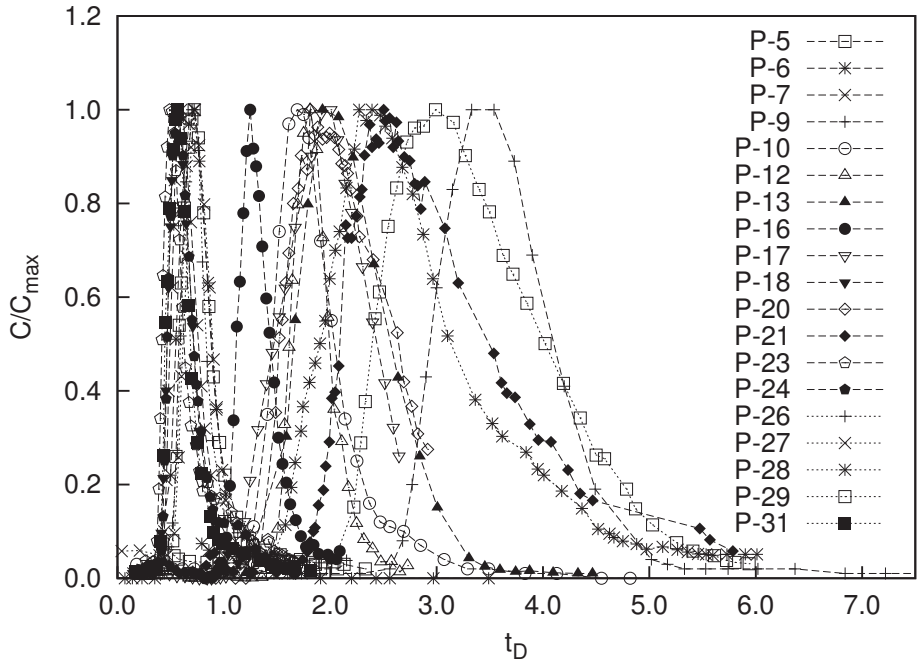

Figure 2.4: Normalized breakthrough curves obtained at different injection location: t_D is the dimensionless time ($t_D = Qt/\pi r^2 b\phi$), where Q is the pumping rate, r the distance from the well, b the aquifer thickness and ϕ the actual porosity. In a homogeneous media all curves should superimpose.

ble. Water is extracted at a constant rate and the flow system is considered at quasi-steady-state (drawdown gradients do not change in time).

Considering that the spatial variability of transmissivity occurring in all natural aquifers is the dominant variable responsible for the existence of preferential flow channels in the system, we view transmissivity as the only varying property in space. The storage coefficient (S) and the effective porosity (ϕ) are assumed spatially constant in the analysis. This is a common workable assumption in stochastic subsurface hydrology since the spatial variability of T is orders of magnitude larger than that of S and ϕ.

Transport point-to-point connectivity involves those physical properties by which the characteristic advective time between the pumping well and the observation location is enhanced or

reduced relative to that of a homogenized equivalent system. Thus, we start by analyzing the advective travel time of a non-reactive mass particle, t_a, injected instantaneously into the system,

$$t_a = \int_\Gamma \frac{\phi}{\|\mathbf{q}\|} ds, \tag{2.7}$$

where Γ is the trajectory of the injected particle, ϕ is the effective porosity (ratio of mobile aqueous phase volume to the total volume), and $\mathbf{q}$ is the Darcy's velocity. Assuming that the particle pathline does not significantly deviate from the mean fluid motion we can parameterize (2.7) using a radial coordinates system centered at the pumping well

$$t_a(r_i, \theta_i) = -\phi \int_{r_w}^{r_i} \frac{1}{q_r(r, \theta(r))} dr. \tag{2.8}$$

In (2.8) (r_i, θ_i) denotes the radial coordinates of the injection location, r_w is the pumping well radius, and q_r is the radial component of the Darcy's velocity,

$$q_r(r, \theta) = -e^Y \frac{\partial h}{\partial r}, \tag{2.9}$$

where $Y(\mathbf{x}) = \ln T(\mathbf{x})$, and h is the drawdown which is in turn governed by the following partial differential equation,

$$\nabla Y(\mathbf{x}) \nabla h(\mathbf{x}, t) + \nabla^2 h(\mathbf{x}, t) = e^{-Y} S \frac{\partial h(\mathbf{x}, t)}{\partial t}. \tag{2.10}$$

Here, S is the true storage coefficient of the aquifer (released pore-water per unit area of the aquifer and unit decline of the piezometric head), assumed also spatially constant. Equation (2.10) is strictly valid only in confined aquifers, but it can be a valid approximation in unconfined aquifers whenever the drawdown is small with respect to the initial saturated thickness. In the presence of

a pumping well, the corresponding boundary and initial conditions are written as,

$$h(\mathbf{x}, t = 0) = 0, \tag{2.11}$$

$$h(|\mathbf{x}| \to \infty, t) = 0, \tag{2.12}$$

$$\lim_{r \to r_w} \left(2\pi r \frac{\partial h}{\partial r} \right) = Q_w e^{-Y_0}, \tag{2.13}$$

where Q_w is the pumping rate per unit of thickness $[m^3/m \cdot day]$. Quasi-steady-state conditions are achieved at large times. Since $Y(\mathbf{x})$ is randomly varying in space, it is in general not possible to obtain analytical solutions of t_a from (2.8). To overcome this problem, we used perturbation theory to find an approximate solution. The approach starts by writing t_a and h in an expansion series,

$$t_a = t_a^{(0)} + t_a^{(1)} + t_a^{(2)} + ..., \tag{2.14}$$

$$h = h^{(0)} + h^{(1)} + h^{(2)} + ... \tag{2.15}$$

The leading terms $t_a^{(0)}$ and $h^{(0)}$ are the solutions of two deterministic problems obtained by substituting the heterogeneous Y-field by an equivalent log transmissivity, $Y_0 = \ln T_0$. The other terms, $t_a^{(i)}$ and $h^{(i)}$ (i=1,2,...), are solutions of stochastic partial differential equations describing the deviations from the homogeneous solution. These terms are of the order of some characteristic scalar value, usually taken as the standard deviation of the natural log of hydraulic conductivity, σ_Y. Thus for small σ_Y the higher order terms, $t_a^{(i)}$ and $h^{(i)}$, become successively less important.

Keeping only the first two terms in the expansion, we write

$$q_r(\mathbf{x}) = q_0(r) + q'_r(\mathbf{x}) \tag{2.16}$$

Taylor expansion around (r, θ_i) yields

$$t_a(r_i, \theta_i) = \\ -\phi \int_{r_w}^{r_i} \frac{1}{q_0(r)} \left(1 - \frac{q'_r(r,\theta_i)}{q_0(r)} + \left(\frac{q'_r(r,\theta_i)}{q_0(r)}\right)^2 + \frac{\partial q'_r(r,\theta_i)}{\partial \theta}(\theta - \theta_i) + ...\right) dr \tag{2.17}$$

By setting

$$Y(\mathbf{x}) = Y_0 + Y'(\mathbf{x}), \tag{2.18}$$

Y_0 being a representative mean value of Y (e.g. the arithmetic mean), and introducing (2.15) into Darcy's law (2.9), and using the Taylor expansion of $\exp(Y')$ we obtain

$$\begin{aligned} q_r(r,\theta) &= -T_0 \left(1 + Y' + \frac{Y'^2}{2} + ...\right) \frac{\partial}{\partial r}\left(h^{(0)} + h^{(1)} + ...\right) \\ &= -T_0 \left(\frac{\partial h^{(0)}(r)}{\partial r} + \frac{\partial h^{(0)}(r)}{\partial r} Y'(r,\theta) + \frac{\partial h^{(1)}(r,\theta)}{\partial r}\right) + ... \end{aligned} \tag{2.19}$$

The first term on the right-hand-side of (2.19) is $q_0(r)$, which is the solution for a radial flow system in homogeneous medium,

$$q_0(r) = -T_0 \frac{\partial h^{(0)}(r)}{\partial r} = -\left(\frac{Q_w}{2\pi}\right)\frac{1}{r}. \tag{2.20}$$

Subtracting the homogeneous solution $q_0(r)$ from $q_r(r,\theta)$ we obtain

$$q'_r(r,\theta) = q_0(r)Y'(r,\theta) - T_0\frac{\partial h^{(1)}(r,\theta)}{\partial r} + ... \tag{2.21}$$

Thus, the Darcy's velocity deviations from the equivalent homogeneous solution depend on the transmissivity field and also on the space distribution of the piezometric head. The solution of the terms $h^{(i)}$ can be obtained using an iterative procedure. We refer to the work of *Sanchez-Vila et al.* [83] for the actual derivation of the solution. Considering a small well diameter ($r_w \to 0$), the first order term is given by

$$\frac{\partial h^{(1)}(r,\theta_i)}{\partial r} = \frac{Q_w}{4\pi T_0}\frac{\partial}{\partial r}\left(-\frac{1}{\pi}\int_V Y'(\rho,\varphi)\, U(r,\theta_i,\rho,\varphi)\, dV\right). \tag{2.22}$$

Combining (2.3) and (2.22) we obtain

$$\frac{\partial h^{(1)}(r,\theta_i)}{\partial r} = \frac{Q_w}{4\pi T_0}\frac{\partial}{\partial r}\left(\ln\frac{S_{est}(r,\theta_i)}{S}\right). \tag{2.23}$$

The term $\ln S_{est}(r,\theta)/S$ in (2.23) is the departure of the estimated storage coefficient (calculated by the Cooper-Jacob method) from the actual coefficient S.

Considering again $r_w \to 0$, we derive the relationship between the characteristic advective travel time, t_a, and the estimated storage coefficient, S_{est}, by simply substituting (2.23) and (2.20-2.21) into (2.17) and integrating by parts,

$$t_a(r_i,\theta_i) = \frac{\phi\pi r_i^2}{Q_w}\left(1 - \int_0^{r_i}\frac{2r}{r_i^2}\left\{Y'(r,\theta_i) - \ln\frac{S_{est}(r,\theta_i)}{S_{est}(r_i,\theta_i)}\right\}dr\right). \tag{2.24}$$

The term $\ln S_{est}(r,\theta_i)/S_{est}(r_i,\theta_i)$ in (2.24) denotes the departure of the estimated storage coef-

ficient at a given point (r, θ_i) located between the injection and the pumping well with respect to the estimated storage coefficient at the injection location (r_i, θ_i).

The series expansion in (2.24) is truncated at the first-order in σ_Y. In an attempt to overcome the latter truncation, we view (2.24) as the first two terms of an exponential expansion and we generalized the final solution as

$$t_a(r_i, \theta_i) = \frac{\phi \pi r_i^2}{Q_w} \exp\left(- \int_0^{r_i} \frac{2r}{r_i^2} \left\{ Y'(r, \theta_i) - \ln \frac{S_{est}(r, \theta_i)}{S_{est}(r_i, \theta_i)} \right\} dr \right). \tag{2.25}$$

This exponentiation is a widely used procedure in stochastic subsurface hydrology [e.g., 34]. Otherwise, the estimation of t_a through (2.24) may yield negative values, which are not physically correct. Recalling (2.5), this last expression can be written in terms of the estimated porosity obtained from interpreting concentration breakthrough curves of convergent flow tracer tests:

$$\phi_{est}(r_i, \theta_i) = \phi \exp\left(- \int_0^{r_i} \frac{2r}{r_i^2} \left\{ Y'(r, \theta_i) - \ln \frac{S_{est}(r, \theta_i)}{S_{est}(r_i, \theta_i)} \right\} dr \right) \tag{2.26}$$

Here, the inverse of ϕ_{est} is viewed as an indicator of transport point-to-point connectivity because it essentially depends upon travel time, which is directly controlled by connectivity. In the homogeneous case, $Y' = 0$, $\ln S_{est} = S$, and thus $\phi_{est} = \phi$. In agreement with field and lab observations, (2.26) demonstrates that in heterogeneous media the estimated porosity ϕ_{est} from a tracer test depends not only on ϕ (actual porosity), but also on Y' and S_{est} along the line connecting the pumping and the injection wells. Thus, ϕ_{est} is not a physical parameter but rather a value coming from the test interpretation method.

In (2.26) we can view $2r/r_i^2$ as a weighting function, increasing linearly from the well to the injection point. Close to the well, the information provided by Y' and S_{est} does not provide any additional information on ϕ_{est}, since the weighting function is almost null. This is logical, since the travel time to the well is not affected by the actual measurements taken at the well location

[81]. On the contrary, largest weights are given to the values corresponding to points located close to the injection location. It should also be noted that S_{est} in turn depends on a spatial average of Y' that extends throughout the entire system (Equation 2.3) and is characterized by a different weighting function, U (Equation 2.4). This function is maximum along the line defined by the pumping and the observation wells, and largely weights the region nearby the two wells [83].

The final ϕ_{est}/ϕ outcome is the balance of two processes. Whenever the transmissivity values along the particle path are larger than T_0 (equivalent field transmissivity), $Y' > 0$ and the first term in (2.26) tends to yield ϕ_{est} values below the representative value of porosity, ϕ. This term directly depends on the transmissivity features between the pumping well and the injection location but does not include direct information on the hydraulic head response induced by pumping. All this information is provided by the second term in (2.26), that expresses that whenever the hydraulic response along the particle path are faster (small S_{est}) than that of the injection location, $(\ln S_{est}(r, \theta_i)/S_{est}(r_i, \theta_i) < 0)$, the second term also tends to decrease ϕ_{est}, and thus increase transport connectivity.

2.4 Computational Investigations

2.4.1 Exploring the Applicability of the Analytical Solution

The robustness of the analytical solution and the relative importance of the variables involved in (2.26) is examined in this section. To achieve this, we numerically generated transport point-to-point connectivity maps in a given synthetic aquifer. We consider the same transmissivity field as used by *Sanchez-Vila et al.* [83] and reproduced here in Figure 2.5a. The computational domain consists of 500 × 500 cells, each of 1 m × 1 m. The log of the transmissivity field, $Y(\mathbf{x})$, corresponds to one individual unconditional realization of a multiGaussian random function characterized by an isotropic spherical variogram model with zero mean, unit variance, and integral scale of 10 m.

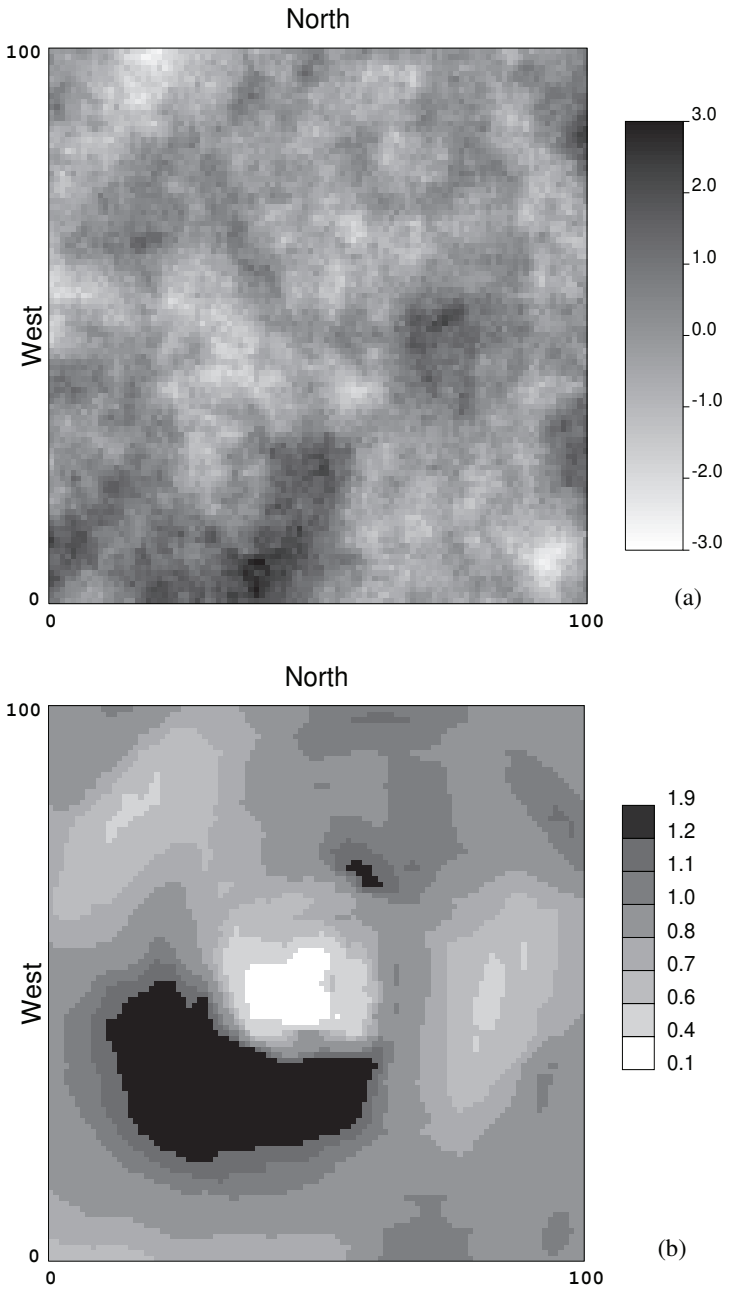

Figure 2.5: Natural logarithm of the transmissivity field (a) and map of S_{est}/S for the given aquifer (b), modified from *Sanchez-Vila et al.* [83]. Each map is representative of a subdomain of 101 × 101 cells centred around the well.

An abstraction well was located at the center of the domain with prescribed flow rate, whereas zero drawdown was fixed at the external boundaries. The domain was artificially enlarged to avoid boundary effects. In this context, *Sanchez-Vila et al.* [83] numerically calculated the spatial variability of S_{est} estimates by simulating the drawdown curves for all nodes of the corresponding groundwater flow model. Their results are shown in Figure 2.5b for comparative purposes.

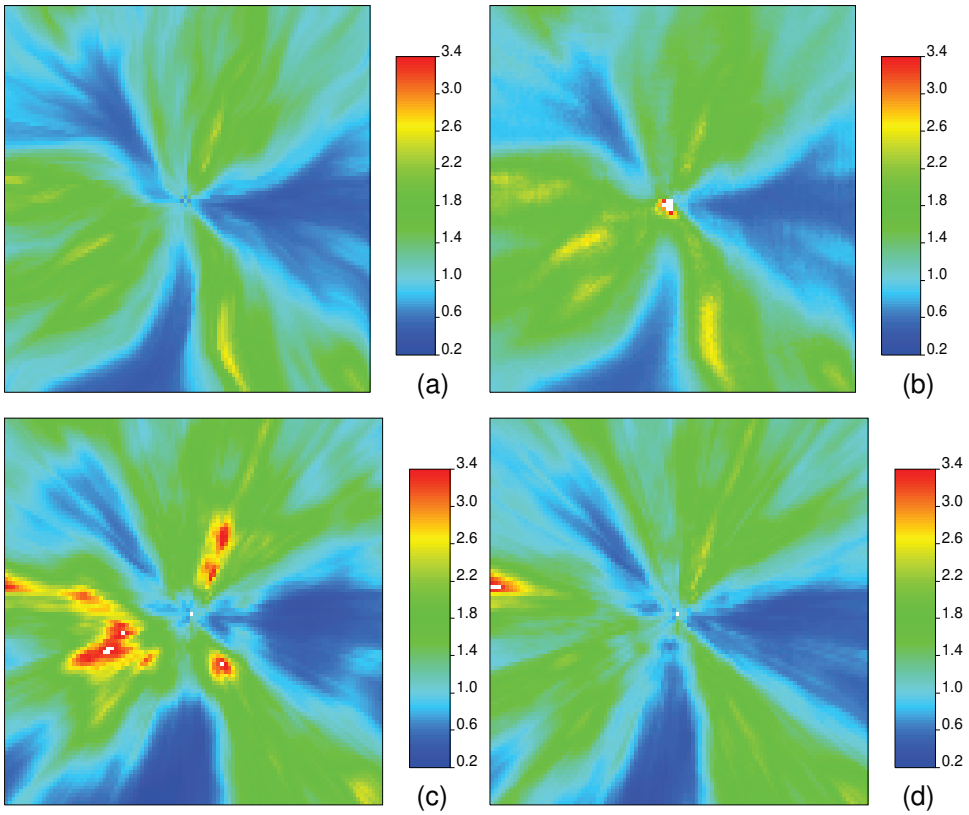

Figure 2.6: Estimated porosity, ϕ_{est} in each cell of a subdomain of 101 × 101 cells centred around the well. The porosity is computed (a) numerically using a purely advective model and (2.5), (b) numerically using an advection-dispersion model and (2.5). The values are compared with ϕ^I_{est} (c) from Equation (2.27) and ϕ_{est} (d) from Equation (2.26). All values are normalized by ϕ.

Here, we generate point-to-point transport connectivity maps by means of the indicator $\phi_{est}(\mathbf{x})$. Each $\phi_{est}(\mathbf{x})$ value is obtained by injecting a slug of mass into the system (at the $\mathbf{x}$ location), solving the corresponding transport problem and then using (2.5). The process was repeated for each grid

cell in the domain.

First, we simulated steady-state flow in this setup using the finite difference code MODFLOW2000 [46]. The resulting velocity field was used to simulate solute transport, which is solved using a random walk particle tracking code, RW3D [30]. For each injection, the characteristic advective travel time was simulated in two ways: (a) using a purely advective model in which only a single particle is injected at the centroid of the grid cell to calculate t_a through (2.7); and (b) using and advective-dispersive model with 100 particles initially uniformly distributed within each cell. In this case, the characteristic advective travel time was estimated by the mean value of all the particle travel times recorded at the pumping well. The longitudinal and transverse dispersivity were set to 1 m and 0.1 m, respectively.

Figures 2.6a and 2.6b show the maps of $\phi_{est}(\mathbf{x})$ for the two different conceptual transport models. We see that connectivity patterns were not substantially changed when including local dispersion processes into the transport model. This indicated that in this particular case, i.e., forced-gradient conditions induced by a pumping well in a continuous porous medium, point-to-point connectivity patterns measured by the advective travel time did not inherit the same stability problems as those observed for aquifers with high conductivity contrasts and under non-convergent flow conditions [98].

In order to evaluate the relative importance of the different processes governing (2.26), we used a new estimate for ϕ given by neglecting all the terms depending on S_{est} in (2.26)

$$\phi^I_{est}(r_i, \theta_i) = \phi \exp\left(- \int_0^{r_i} \frac{2r}{r_i^2} Y'(r, \theta_i) dr \right) \tag{2.27}$$

Then, we compare the results given by (2.27) with those obtained from the numerical simulation of $\phi_{est}(\mathbf{x})$. The approximate solution (2.27) was computed considering $Y'(\mathbf{x}) = \ln T(x)/T_g$. Comparison of Figure 2.6a and 2.6b with Figure 2.6c shows that $\phi^I_{est}(\mathbf{x})$ can still capture those zones well connected (low ϕ_{est} values) with the pumping well, altough the size of the well con-

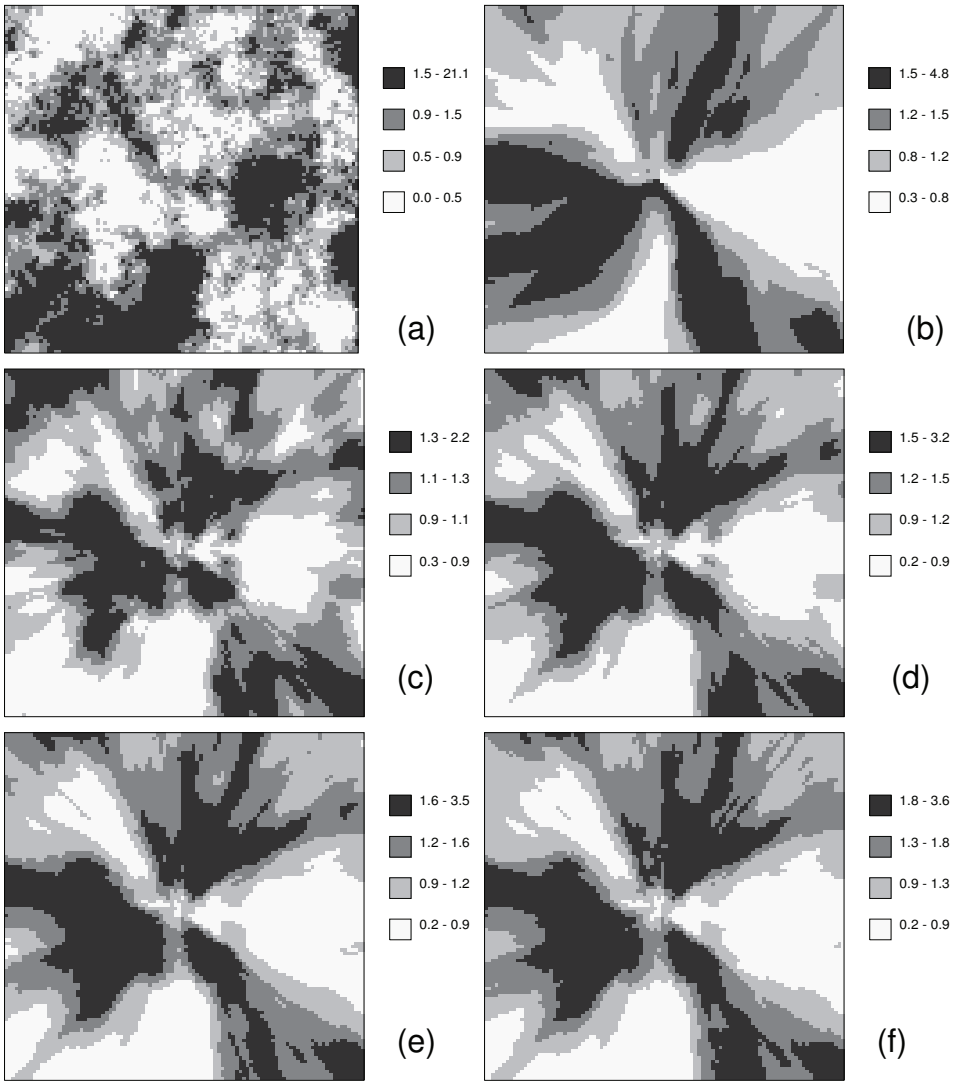

Figure 2.7: (a) Transmissivity field, (b) porosity estimated numerically using Equation (2.5), porosity estimated ϕ_{est}^{II} using Equation (2.28) with (c) $\alpha = 1/4$, (d) $\alpha = 1/2$, (e) $\alpha = 2/3$ and (f) $\alpha = 1$. Each map is representative of a subdomain of 101×101 cells centred around the well.

nected zone to the south is slightly overestimated. The poorly connected zones (high ϕ_{est} values) are still delineated by $\phi_{est}^{I}(\mathbf{x})$, although in this case the size and the degree of connectivity is overestimated.

The complete analytical solution (2.26) incorporates not only the values of $Y'(\mathbf{x}) = \ln T(x)/T_g$

but also the hydraulic response of the system through $S_{est}(\mathbf{x})$ (second term) whose values are borrowed from those numerically computed by *Sanchez-Vila et al.* [83] (Figure 2.5b). Comparison of Figures 2.6a and 2.6b with Figure 2.6d illustrates that the $S_{est}(\mathbf{x})$ term improves the delineation of zones of low to moderate connectivity while has a minor impact on the depiction of the fastest channels. We note that albeit the complete analytical solution (2.26) in Figure 2.6d compares favorably with numerical simulations, the connectivity patterns delineated using both analytical solutions (Figure 2.6c and 2.6d) are slightly less tortuous than those obtained numerically (Figures 2.6a and 2.6b) probably because of the first order truncation of (2.21).

We highlight the striking difference between both indicators of point-to-point connectivity: $\phi_{est}(\mathbf{x})$ (transport connectivity) and $S_{est}(\mathbf{x})$ (flow connectivity) (compare figures 2.6d and 2.5b respectively). While the $S_{est}(\mathbf{x})$ map (Figure 2.5b) indicates a poor hydraulic response (black pixels) in the southern part of the domain, $\phi_{est}(\mathbf{x})$ is still well connected with the pumping well since large values of transmissivity are encountered in that region (Figure 2.6d).

Equation (2.27) relates the transmissivity values located along the line between the pumping well and the injection point to the estimated porosity. These transmissivity values are averaged by a linear weighting function that ranges from $2/r_i$ at the injection location to zero at the well. This means that the influence of the T-values decreases as the particle travels towards the well where extreme gradients occur. From this consideration, it is worthwhile to assess the reliability of (2.27) when only a part of the T-values is used. This is achieved by examining the following approximation of $\phi_{est}(\mathbf{x})$,

$$\phi^{II}_{est}(r_i,\theta_i) \approx \phi \exp\left(-\int_{r_i-\alpha r_i}^{r_i} \frac{2r}{r_i^2} Y'(r,\theta_i)dr\right) \tag{2.28}$$

where α is a constant ranging from 0 to 1. Here, for simplicity, we divided the results in quartiles that could correspond to classes of connectivity (low, moderate, good, high). Figure 2.7 shows the numerical simulation of (2.28) when $\alpha = 1/4, 1/2, 2/3, 1$. Using the information con-

tained in only one-fourth of path-line, i.e. $\alpha = 1/4$, the approximation is still strongly influenced by the transmissivity at the injection location. This is the reason for Figure 2.7c to have a similar shape as the transmissivity field (Figure 2.7a). Using $\alpha = 1/2$ the approximation is able to capture three well connected zones with the pumping well (east, north-west and south-west). Zones poorly connected are not so well delineated, mainly because (2.28) does not include the term in (2.26) involving the S_{est} values. The use of the information located in the last half of the line, (that are included using $\alpha = 2/3$ and $\alpha = 1$) leads to a very small improvement in the results (figures 2.7e and 2.7f).

2.4.2 Comparison with Laboratory Tracer Experiments

Here, we assess the analytical solution (2.26) against the intermediate-scale laboratory tracer experiments detailed in section 2.2.1. We note that the transmissivity field in this case depicts a non-multiGaussian field in that extreme (low and high) values of transmissivity exhibit significant correlation. Since no hydraulic test information was reported for the experiments, we only evaluated the behavior of ϕ^I_{est}, i.e., we neglected the second term in (2.26), whose influence we showed to be limited to the delineation of low connectivity areas. Figure 2.8 compares the natural log of ϕ^I_{est} values determined by (2.27) with the corresponding experimental values. The true porosity of the system used in (2.27) was obtained gravimetrically from core samples and is $\phi = 0.44$ [29]. The equivalent transmissivity, T_0, was set equal to the arithmetic mean ($21 m^2/day$). This value was determined by best fitting the experimental travel times, ϕ_{est}, with their corresponding values. T_0 is close to the arithmetic mean probably because the aquifer system is well stratified. The results are shown in Figure 2.8 and give a satisfactory linear correlation coefficient ($r^2 = 0.75$) between the analytical solution and the experimental data. It must be noted that the calibration of T_0 would only affect the y-intercept of the regression line, having no influence in the linear correlation coefficient.

The comparison with the analytical solution (Figure 2.8) is less accurate for ports P13 and P24.

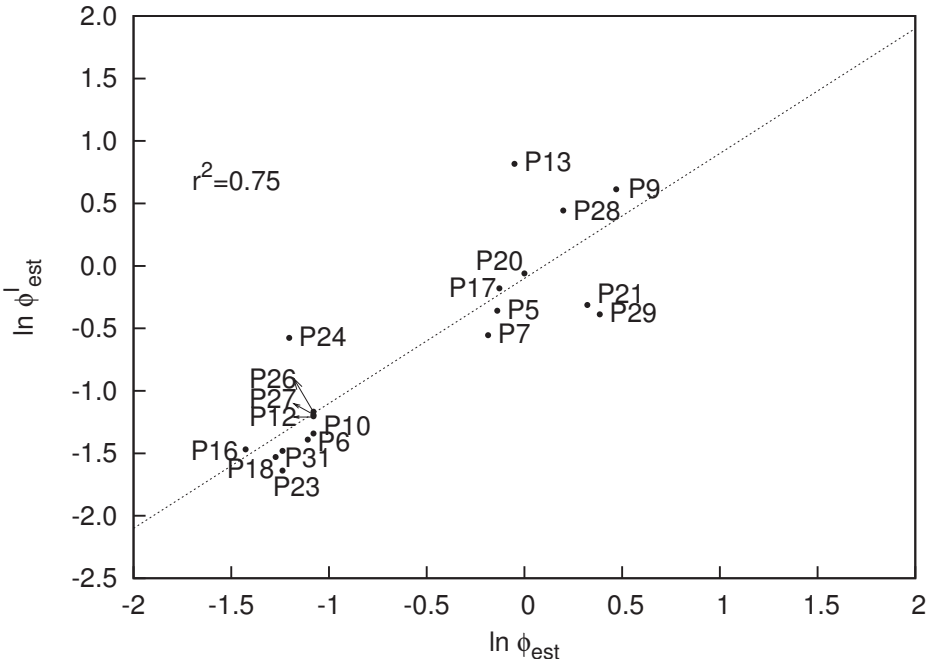

Figure 2.8: Natural logarithm of the estimated porosity from laboratory, $\ln \phi_{est}$, versus the natural logarithm of the transmissivity estimated using Equation (2.27) ($\ln \phi^I_{est}$). The linear trendline and the correlation coefficient (r^2) are indicated.

Based on the lab estimated porosity values, we note that these ports are located within, or close to, areas of poor point-to-point connectivity, which is consistent with the fact that ϕ^I_{est} overestimates ϕ_{est} in poorly connected areas (section 2.4.1). The poor agreement observed in P21 and P29 can be attributed to boundary effects since both ports are located close to the limits of the domain.

2.5 An Application: Delineation of capture zones

The definition of protected areas, where anthropogenic activities are limited, is a key issue for the safeguard of water resources. Being economically and socially unfeasible to protect the entire aquifer, protection actions typically focus on small areas around the abstraction wells. As an example, the European Water Framework Directive requires the establishment of safeguard zones

leaving to the discretion of the member state the methodology to identify these areas. Nonetheless, in the guidance document on groundwater in drinking water protection areas [13], it is explicitly mentioned the 'time of travel to the abstraction' as a factor influencing the size and the shape of the capture zone. In this context, the impact of point-to-point transport connectivity on the identification of capture zones is of paramount importance. The mathematical framework and companion numerical simulations presented here give insight into the concept of transport connectivity which can be used to improve standard methodologies devoted to the delineation of capture zones.

To illustrate this, we use the analytical and simplified solutions (2.26) and (2.27) to delineate the protection perimeter around the abstraction well used in the synthetic aquifer of section 2.4.

The protection perimeter was defined so that any accidental spill in a point located out of the perimeter will take more than 50 days to reach the pumping well. We adopted the same parameters as those given in section 2.4, having a pumping rate of $Q_w = 30\ m^3/m \cdot day$.

The capture zone obtained using the analytical solution was compared with numerical backward simulations. One thousand particles were injected at the well and backtracked to compute their position after 50 days. Two conceptual transport models were used. A purely advective transport model and an advective-dispersive model with longitudinal and transverse dispersivity set to $1m$ and $0.1m$, respectively.

Figure 2.9a show the result of the purely advective model and clearly exhibits that the analytical solutions closely follow the numerical simulation results, thus capturing the most important connectivity features. For comparison purposes, these results are also contrasted with those associated with an equivalent homogeneous medium obtained by substituting the heterogeneous T-field by a homogeneous one. We see that the extension of the capture zone stretches over or falls inside the homogeneous perimeter in those parts of the domain with high and low connectivity, respectively. Thus, disregarding the role of connectivity induces a bias in the delineation of the capture zone in such a way that the size of well connected areas with the pumping well is underestimated.

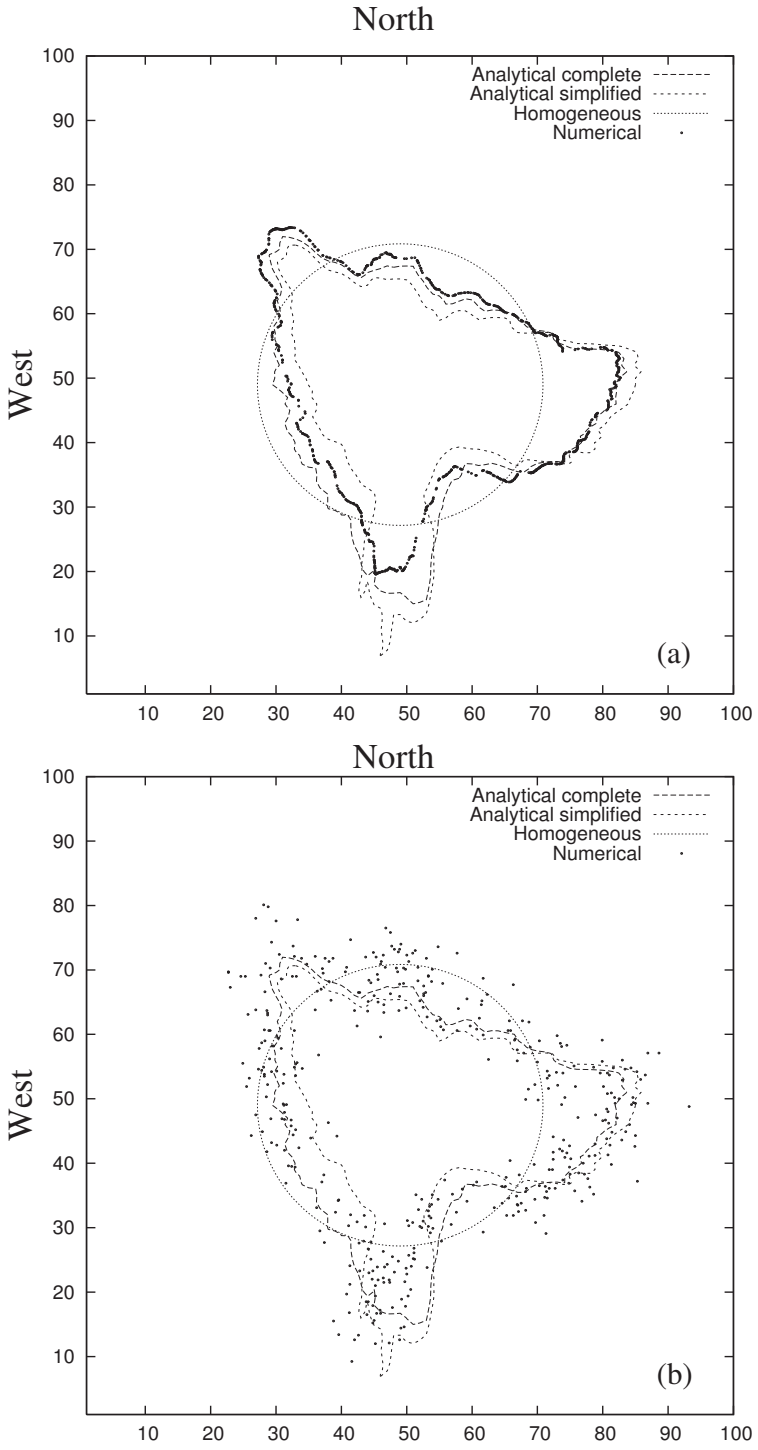

Figure 2.9: Identification of the 50 days travel time capture zone from a well located at $(50, 50)$. The numerical results have been obtained with backward simulations using (a) a purely advective model and (b) an advection-dispersion model. The analytical complete and simplified solutions refer to Equation (2.26) and (2.27) respectively.

In agreement with section 2.4, the simplified analytical solutions (2.27) depicted in Figure 2.9 tends to overestimate the size and the degree of poorly connected zones. Highly connected areas are slightly overestimated with the exception of the northern zone (slightly underestimated).

The thousand particles of Figure 2.9b show the backward location probability density function (PDF) which describes the position of the contaminant at a fixed time (50 days) prior to its recovery at the well. The perimeter delineated using (2.26) agrees quite well with the mean shape (50% probability) of the particles cloud.

2.6 Summary and conclusions

We present an explicit mathematical framework that assesses the meaning of point-to-point connectivity in heterogeneous aquifers through the study of two commonly used indicators of connectivity (S_{est} and ϕ_{est}). The analysis focuses on the impact of connectivity features on solute transport behavior under a radially convergent flow system. Our analysis leads to the following main conclusions:

1. We have theoretically demonstrated that the estimated porosity, ϕ_{est}, obtained from field tracer tests is an indicator of point-to-point transport connectivity rather than related to the total void volume of the aquifer. When the pumping well is hydraulically well/badly connected with a given location, ϕ_{est} takes values below/above the representative porosity of the aquifer.

2. This indicator of connectivity, ϕ_{est}, involves two terms. The first term depends on the transmissivity values located along the flow path line such that large transmissivity values, i.e., larger than the equivalent homogeneous transmissivity of the aquifer, leads to estimates of ϕ_{est} smaller than ϕ and vice versa. The second term incorporates the hydraulic response of the aquifer (flow connectivity) induced by pumping, which is measured by the estimated storage coefficient, S_{est} (calculated by the Cooper-Jacob method) defined by the observation point moving along the same path line. Point-to-point transport connectivity gets amplified/reduced when the time of the

hydraulic response along the flow path line decreases/increases in the direction of flow. Both terms are weighted by a function that increases linearly with the radial distance from the pumping well. Thus, transport point-to-point connectivity is largely influenced by the aquifer properties close to the injection location, while transmissivity or S_{est} data at points located nearby the pumping well provide no information on ϕ_{est}.

3. We have theoretically demonstrated that the underlying processes governing transport connectivity are distinct from those involved in flow connectivity. The indicator of flow connectivity S_{est} can be viewed as a weighted averaged over the entire domain, while the indicator of transport connectivity ϕ_{est} is a weighted averaged along the flow path line. Moreover, the transport weighting function (proportional to the radial distance) is remarkably different from that of flow connectivity, the latter assigning large weights to all the points located between the observation and the pumping well.

4. Comparison of the analytical solution of ϕ_{est} with numerical simulations performed in a given synthetic heterogeneous aquifer show that our mathematical framework is able to delineate low and high connectivity patterns with a good approximation in moderately heterogeneous aquifers. In particular, we found that the relative contribution of the hydraulic response (S_{est}) to transport connectivity (ϕ_{est}) is minor, causing only a slight overestimation of low connectivity patterns. It is worthwile to note that the analytical solution is obtained from a truncated perturbation expansion. Its accuracy in highly heterogeneous media should be explored in the future.

5. Delineation of point-to-point transport connectivity requires a limited amount of information since it mostly depends only on the transmissivity point values along the flow path line (minor contribution of S_{est}), being redundant the information nearby the well because of the shape of the transport weighting function.

6. The analytical solution of ϕ_{est} (2.27) was successfully contrasted with laboratory tracer experiments conducted in a reconstructed heterogeneous anisotropic medium with high correlation

of extreme values (non-multiGaussian patterns). Results were consistent with our previous numerical observations. Well connected features were successfully captured by the analytical solution while the size and degree of low connectivity patterns were slightly overestimated.

7. The role of connectivity is seen to be of paramount importance for the delineation of protection areas (i.e. capture zones). Areas well connected with the pumping well exhibited protection perimeters that stretched beyond the equivalent homogeneous solution, i.e., the perimeter obtained considering a homogeneous aquifer. In this context, we present a novel simplified procedure to estimate the protection area of an abstraction well while honoring connectivity patterns. The methodology was successfully applied to a synthetic heterogeneous aquifer.